Earth and Planetary Science Letters, 110 (1992) 77–94
Elsevier Science Publishers B.V., Amsterdam

[UC]

Internal circulation in a buoyant two-fluid Newtonian sphere: implications for composed magmatic diapirs

Roberto Ferrez Weinberg

The Hans Ramberg Tectonic Laboratory, Institute of Geology, University of Uppsala, 751 22 Uppsala, Sweden

Received November 11, 1991; revision accepted March 4, 1992

ABSTRACT

Igneous plutons frequently show chemical zoning. The most commonly documented zoning is with the lighter, more silicic, rocks in the centre of the body and the denser, more basic, rocks in the external zone (normal zoning). Less commonly, some plutons show reverse zoning so that the more basic rocks occupy the centre. Widespread evidence shows that zoning in many plutons is the result of interaction between basic and silicic melts.

This work studies, by means of finite difference numerical models, pluton zoning which is due to internal circulation in diapirs comprising two magmas of different composition. Diapirs are modelled here as buoyant isothermal spheres composed of two Newtonian fluids rising through a Newtonian ambient fluid. Ratios of viscosities and densities of the two fluids were varied and the results demonstrated two different styles of internal circulation in rising spheres. The first style, termed "coupled circulation", is characterised by continuous overturning of both the fluids in a single cell, evolving through both normal and reverse compositional zoning. The overturns stir the fluids and enhance both magma mingling and mixing. Coupled circulation develops in spheres comprising fluids of similar densities and viscosities. As these properties become increasingly different the internal circulation tends to decouple. "Decoupled circulation", is characterised by circulation of the fluids in two separate cells. Decoupling stops the overturns between the two magmas so that the diapir preserves a reverse zoning throughout its rise, with the denser fluid occupying the central zone. There is less possibility of magma mingling in diapirs undergoing decoupled circulation. Thus, pairs of magmas of similar properties, such as andesite and rhyolite, are most likely to develop coupled circulation leading to both normal and reverse zoning in diapirs; whereas magmas of very different properties, such as basalt and rhyolite, are most likely to decouple resulting in reverse zonation.

The models indicate that reverse zoning would be the most common internal pluton geometry if zoning were controlled by internal circulation alone. Model diapirs which rise along channels of warm, low viscosity wall-rock (hot Stokes' models) or low viscosity shear zones show an increased tendency towards coupled circulation and more intense mechanical stirring of the magmas.

Introduction

Widespread evidence suggests that mantle basalts trigger melting of the silicic crust leading to plutons initially composed of two distinct melts [1,2]. This association is often observed in the form of mechanical mingling and chemical mixing of the two magmas in zoned plutons or as mafic enclaves in granitoids (e.g. [3,4]). The most commonly described pattern of compositional zoning in granitoid plutons—normal zoning—is characterised by mafic margins around felsic cores (e.g. [5,6]). Felsic margins around mafic cores—reverse zoning—are considered to be less common (e.g. [4,7–9]). Several mechanisms have been proposed for compositional zoning in plutons. Some models suggest mechanisms, such as differentiation during crystallization, thermal convection, and crystal settling [10] that occur after the pluton has been emplaced at high crustal levels. The models considered here suggest that zoning is caused by mechanisms related to pluton ascent and offer alternative answers to several questions regarding this zoning [11]. The present work investigates the possibilities of zoning due to internal circulation caused by diapiric ascent of bi-

Correspondence to: R.F. Weinberg, The Hans Ramberg Tectonic Laboratory, Institute of Geology, University of Uppsala, Box 555, 751 22 Uppsala, Sweden.

modal plutons, or by diapirs rising from a deep, differentiated magma chamber [9]. The ascent of these composite diapirs was simplified to a buoyant isothermal sphere (following [12–16]) containing two immiscible Newtonian fluids. The patterns of internal circulation in the sphere caused by the viscous drag by its surroundings were studied by means of finite-difference numerical models.

This paper opens with a short summary of previous research, followed by a description of the methods used for the numerical models. The results are then used to distinguish two styles of internal circulation: coupled and decoupled circulation (Fig. 1). The physical parameters of the fluids were systematically varied in the numerical models and the effects of each parameter on the internal circulation are described individually. The results are then integrated into a general picture and the implications for magma mixing and mingling [17] are discussed. Following this insight into the parameters controlling the internal circulation and the patterns developed, the results of calculations where a sphere rises along a pathway (channel) of low viscosity ambient fluid are discussed (simplified hot Stokes model). A similar experimental approximation has previously been noted [16]. Channel models are believed to be analogues of low viscosity shear zones, or of diapirs rising along pathways in the crust which have been warmed by preceding diapirs.

Previous research

Grout [18] suggested that magmas can rise by forcefully piercing through their overlying rocks (diapiric ascent). Since the work of Ramberg [19,20] diapirism has been widely used to account for the ascent of magmas through both mantle and crust. Batchelor [21] showed that a fluid sphere moving at a constant low velocity (low Reynolds number) through another fluid will retain its spherical shape during flow. Laboratory models show that diapirs with a viscosity lower than that of the enclosing medium, as is the general case in nature, will achieve an almost spherical shape after rising a distance equivalent to few radii [22]. Similar results have been obtained from numerical analysis [23,24]. Although a sphere is a good approximation of the shape of rising diapirs, several other factors present in natural systems may influence their shapes. These include: the geometry of the source region, superimposed syn-tectonic stresses, density and viscosity stratifications of the surrounding medium, or any other possible inhomogeneities [25].

Several workers have used the structures around granitoid plutons to conclude that the viscosity of the pluton and wall rocks must have been similar during ascent, which, in turn, implies that the granitoids must have been highly crystallized during their Stokes-like ascent [20,26]. Another group of workers follow Grout [18] and suggest that deformation around diapirs occurs within narrow zones thermally softened by the diapir itself [12–15,27]. These "hot Stokes models" consider the temperature dependence of the viscosity of the wall-rock and the Peclet number (Pe) of the system (which gives the ratio between heat advection by diapiric rise relative to heat diffusion to the enclosing medium). Most of the models described here simulate the isoviscous Stokes models, but simplified models of hot Stokes rise were also studied.

Marsh [12] showed that the viscosity of the wall rock near the contact controls the drag imposed on rising diapirs and that, for diapirs to rise considerable distances, the wall rock should attain at least the viscosity corresponding to its solidus. Thus, viscosity contrasts close to unity may be expected across the external boundary of diapirs. The viscosities of felsic and mafic magmas depend on their composition, temperature, pressure, crystallinity and water content [4,17,28,

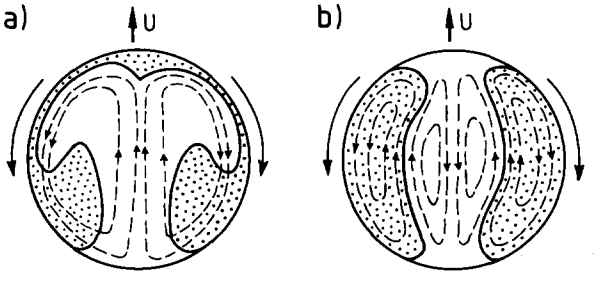

Fig. 1. (a) Coupled internal circulation showing one flow cell in each half sphere. (b) Decoupled internal circulation with two flow cells per half sphere, a very thin skin of the fluid circulating in the core also surrounds the external fluid.

29]. Their viscosity ratio may vary several orders of magnitude and will keep changing as the diapir rises, circulates and cools. The viscosity contrasts between magmas of different compositions at thermal equilibrium have been calculated as a function of the volume of mafic magma in the total volume [4,17].

The steady velocity, ν, reached by a buoyant sphere slowly rising through a Newtonian fluid of infinite extent is given by the extended Stokes' Law for the motion of a sphere [30,31]:

$$\nu = \frac{1}{3}\frac{r^2 g \Delta\rho}{\eta_o}\frac{(\eta_o + \eta_s)}{(\eta_o + \frac{3}{2}\eta_s)} \quad (1)$$

where: r is the sphere's radius; g the gravitational acceleration; $\Delta\rho$ the density difference between the sphere and surrounding medium, and η_o and η_s are the viscosity of the ambient fluid and of the sphere, respectively. The theoretical velocity of the two-dimensional model spheres is found by multiplying eq. (1) by the correcting factor k for an infinite cylinder, $k = 1/0.8488$ [32].

The internal circulation promoted by viscous drag in an isothermal non-expanding fluid sphere moving through an infinite fluid has been studied earlier by several workers [21,25,30,31,33,34]. Schmeling et al. [25] studied this internal circulation using a model of Stokes flow past a fluid sphere, with arbitrary viscosity contrast to the ambient medium. Their results showed that the fluids inside the sphere overturn completely after travelling a distance S_{ov}:

$$S_{ov} = \frac{32r}{3}\frac{(\eta_o + \eta_s)}{\eta_o} \quad (2)$$

Cruden [35] was the first to study internal circulation caused by viscous drag in spheres with an internal density stratification. This author did not notice any retardation of the internal circulation caused by the internal density differences and concluded that any internal stratigraphy behaved passively. However, retardation effects in his experiments may have been small and masked by both difficulties in measuring the circulation rates, and by differences in the volumes of his three internal layers. From the flow inside the diapir, Cruden calculated numerically the time-dependent finite strain developed inside the diapir and predicted the fabrics resulting from such strains. Cruden [35] also emphasised the relevance of internal circulation in diapirs for common features in plutons such as magma mixing and compositional zoning. Magma mixing has been widely described in previous works (e.g. [36]) and Frost and Mahood have shown that magmas of the same viscosity mix the most easily [4].

According to scale model theory, the conditions of geometric, kinematic and dynamic similarity with natural structures must be satisfied so that the model evolves similarly to the prototype [19]. In order to obtain dynamic similarity, the model materials and the natural prototype must also show rheological similarity [37]. Magmas behave as Newtonian fluids above their liquidus temperature and sometimes below [28,29]. Magmas below their liquidus, partial melts and natural rocks all exhibit non-Newtonian behaviour [28,38–42]. Following Ramberg [43] the system will be simplified to an isothermal Newtonian flow in order to gain insight into the principal mechanisms of the problem considered.

All previous studies dealing with internal circulation in buoyant spheres have explored single fluid spheres (e.g. [25,33–35]). The circulation in such a sphere occurs in a single toroidal cell and has been termed here coupled circulation (Fig. 1a). By introducing a second fluid in the sphere, it will be shown that the single cell may disrupt into two decoupled flow cells (decoupled circulation, Fig. 1b), and that the parameters controlling the style of internal circulation are the differences between densities, viscosities and volumes of the two internal fluids.

Numerical models

The two-dimensional numerical models were carried out using a finite-difference computer code developed by Harro Schmeling that solves Stokes equations and was described in Weinberg and Schmeling [44]. The box used had a no-slip bottom boundary, a free-slip top boundary, and reflective lateral boundaries. All calculations used 43×46 grid intersections and 200×200 markers. The width of the box controlled the maximum size of the flow cells caused in the ambient fluid by the rise of the sphere, and was a third of the height and approximately four times the radius

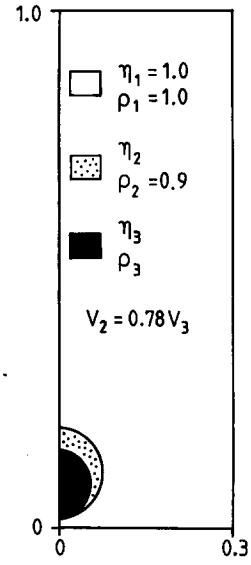

Fig. 2. Initial geometry and physical properties in the numerical models. All boxes were of the width indicated here, and ρ, η, V are the density, viscosity and volume of the fluids, respectively.

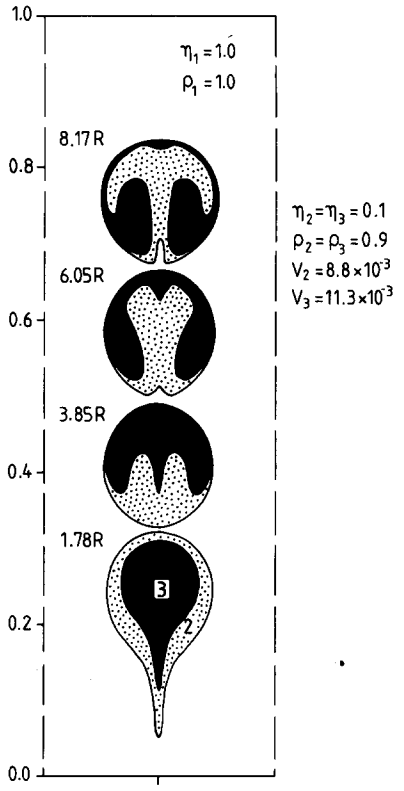

Fig. 3. Reference model where the two internal fluids are of equal density and viscosity. For every step the rise of the sphere is indicated in terms of its radius.

(4r) of the sphere. Batchelor [21] and Marsh [12] pointed out that deformation of the surroundings will propagate many body radii in viscous fluids. In order to evaluate how much the chosen width of the box affected the patterns of internal circulation, a few models were repeated in wider boxes (12r) without significant differences.

In the numerical models described here, viscosity within the fluids are constant and the maximum Reynolds number obtained, $\mathrm{Re} = 10 - 26$, ($\mathrm{Re} = \nu r \Delta\rho / \eta$, calculated for $\nu = 2 \times 10^{-11}$ m/s^2, $r = 2400$ m, $\Delta\rho = 420$ kg/m^3 and $\eta = 2.8 \times 10^{20}$ Pas), is sufficiently small that inertia can be neglected and Stokes' Law can be applied [32]. The computer code has problems dealing with high ($> 10^3$) viscosity contrasts across material boundaries and this limitation constrained the viscosities used in the calculations.

The initial configuration of the numerical models is shown in Fig. 2. The physical parameters of the ambient fluid *1* were kept constant in all models, as well as the relative volumes of the two internal fluids (V_2 and V_3). The patterns of internal circulation were studied by systematically varying the densities and viscosities of the internal fluids (2 and 3, Fig. 2), and delineating the conditions for development of coupled and decoupled circulations. The parameters η_2, η_3 and ρ_3 were varied individually in different sets of calculations while the other parameters were kept constant at the non-dimensional values indicated in Fig. 2. The initial geometry of the sphere was designed to simulate diapirs formed by a batch of basalt melting a smaller volume of silicic crust.

The results of calculations where the two internal fluids, *2* and *3*, have equal density and viscosity (effectively only one fluid) will be used

Fig. 4. Results of model calculations where only density ρ_3 was varied. In the left-hand side box the result of the reference model is shown for comparison and the constant parameters are specified. (a) ρ_3 is decreased and $\rho_2 \geqslant \rho_3$. (b) ρ_3 is increased, as is $\rho_2 \leqslant \rho_3$; notice how the sphere's tail becomes longer and more voluminous as ρ_3 increases.

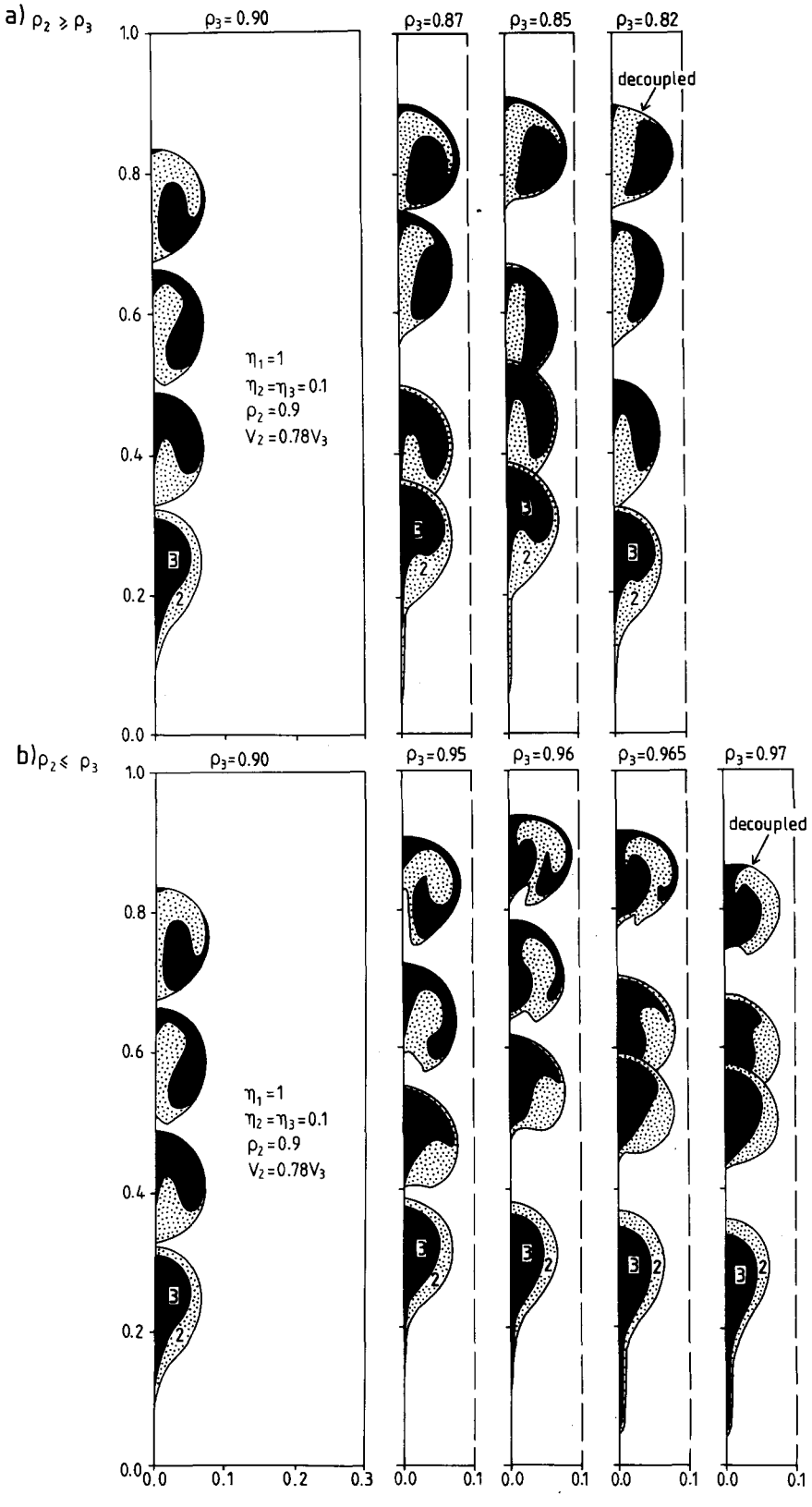
a) $\rho_2 \geq \rho_3$
$\rho_3 = 0.90$
$\rho_3 = 0.87$
$\rho_3 = 0.85$
$\rho_3 = 0.82$
decoupled
$\eta_1 = 1$
$\eta_2 = \eta_3 = 0.1$
$\rho_2 = 0.9$
$V_2 = 0.78 V_3$
b) $\rho_2 \leq \rho_3$
$\rho_3 = 0.90$
$\rho_3 = 0.95$
$\rho_3 = 0.96$
$\rho_3 = 0.965$
$\rho_3 = 0.97$
decoupled
$\eta_1 = 1$
$\eta_2 = \eta_3 = 0.1$
$\rho_2 = 0.9$
$V_2 = 0.78 V_3$
1.0
0.8
0.6
0.4
0.2
0.0
0.0
0.1
0.2
0.3

here as a reference model (Fig. 3). The sphere developed coupled internal circulation as described by Schmeling et al. [25] but similar shapes developed after shorter distances of rise. The top sphere shown in Fig. 3 rose $8.17r$ (r = radius of the sphere). A similar shape was obtained by Schmeling et al. [25] for a sphere rising in an infinite medium only after $11r$ (re-calculated for the viscosity contrast between ambient fluid and sphere used here). The faster development is only apparent and results from the initial geometry used here, which corresponds to a later stage of evolution of the spheres calculated by Schemling et al. [25].

Early acceleration distorts the initial sphere into a teardrop, as a tail is dragged by the enclosing fluid *1* (Fig. 3, bottom diagram). As ascent continues, the velocity becomes constant and the initial spherical shape tends to be regained. The size of the tail is important because the rate of rise (discussed below) depends on the square of the sphere's radius. The models calculated here show that the tail increases in relative volume if the viscosities of fluids *2* and *1* are similar, or if a large density contrast exists within the sphere (Fig. 4).

Density variation

The coupled circulation developed in the reference model (Fig. 3) tended to decouple when the density ρ_3 was varied while keeping ρ_2 constant. Circulation tends to decouple irrespective of whether ρ_3 is smaller than ρ_2 (Fig. 4a) or larger (Fig. 4b). The transition is gradual and, as the density difference increases, an increasing volume of the less dense fluid accumulates in the external zone and remains there over increasingly greater rise distances. For any given set of parameters, there are thus two values of ρ_3 that separate coupled from decoupled circulation, depending on whether the lighter fluid is initially in the centre of the sphere (Fig. 4a) or in the external zone (Fig. 4b). In both cases a high density contrast always leads to decoupling, with the lighter fluid occupying the external zone.

The manner in which the circulation pattern develops depends on the relationship between viscous shear at the sphere's external boundary and the relative buoyancy between the two internal fluids (analogous to the analytical solution of Marsh and Maxey [45] for light particles dragged downwards by flow in a convection cell). When the buoyancy contrast between the two internal fluids is low, viscous shear can drag the lighter fluid downwards around the periphery of the sphere and drive overturns. As buoyancy of the lighter fluid is increased (towards the right-hand side in Fig. 4), it increasingly resists the downward drag, trying to maintain the gravitationally stable stratification. As the buoyancy contrast increases, a point is reached where the initial single flow cell disrupts into two smaller cells. Flow in the two fluids becomes decoupled and circulation occurs inside the fluids' respective boundaries. This situation is stable. Once it is achieved, the relative position of the two fluids remains unchanged throughout the further rise of the sphere. A high-resolution calculation showed a small radius sphere rising 14 radii to the top of the box in a stable decoupled configuration.

When the core fluid *3* is much lighter than the margins, the flow decouples into two cells and the geometry becomes stable after half an overturn (Fig. 4a, right-hand side). On the other hand when the core fluid 3 is denser than the margins, flow can decouple early and stop any overturn. The denser fluid rises towards the top of the sphere during the initial acceleration but the viscous forces driving the circulation are so weak that it sinks down through the core of the sphere (Fig. 4b, right-hand side). In both cases the well known "up through the centre and down around the sides" sense of flow [21,35] breaks down into two separate cells; the sense of flow of the central cell being the reverse of that of the outer cell (Fig. 1b). The case where ρ_3 is denser than the ambient fluid *1* (basaltic magma denser than the crust) was not considered here. However, the tails formed behind the sphere in Fig. 4b allows the prediction that the ascending sphere will leave most of the dense fluid behind, and the internal circulation will be decoupled. The critical density contrasts separating coupled from decoupled circulation are relevant to magmatic processes inside a rising diapir and will be defined later as a function of viscosity.

Viscosity variations

The influence of viscosity variations on the pattern of circulation of a two-fluid rising sphere

was studied by altering the viscosity of one internal fluid while keeping all other parameters constant. Viscosity variations were studied in both fluids of equal density and fluids with different densities. The results show that the viscosity ratio, m (η_2/η_3) between the two internal fluids plays an important role in decoupling internal circulation.

Figure 5 shows the results of model calculations in which the two internal fluids were of the same density and m was varied. The isoviscous sphere of Fig. 5a shows the most coupled circulation. As the internal viscosity contrast varies, internal circulation tends to decouple (Fig. 5b, c). In Fig. 5b the more viscous fluid is in direct contact with the equally viscous ambient fluid (*1*) causing a long tail, trailing behind the sphere, while the two internal fluids overturn. In the inverse initial situation (Fig. 5c), the low viscosity fluid occupies the external zone of the sphere, resulting in a small tail behind the sphere formed by the more viscous internal fluid *3*, and a slower internal overturn as compared to Fig. 5b. The less viscous fluid tends to occupy the external zone of the sphere over greater distances in Fig. 5, as the less dense fluid did in Fig. 4. The differences observed in Fig. 5 contradict earlier observations that viscosity contrasts within the sphere would not affect the structures developed (fig. 1 in [46]) but may be explained by the principle of viscous dissipation [47] which states that two flowing fluids tend to minimise viscous dissipation by arranging the lower-viscosity fluid in regions of higher shear (in this case the external zone of the sphere). The resulting internal circulation pattern is thus an equilibrium between the fluids' ten-

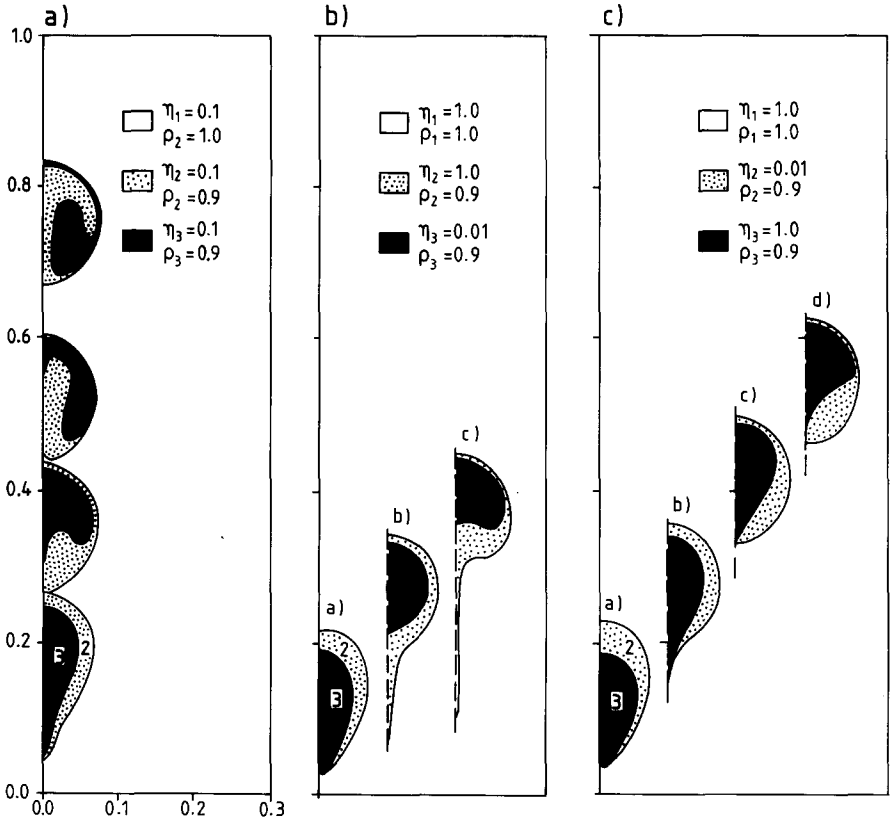

Fig. 5. Calculations for internal fluids with the same density, in which the initial position of the more viscous fluid in the sphere is changed. (a) Isoviscous sphere. (b) With the more viscous fluid in the external zone of the sphere. (c) With the less viscous fluid in the external zone. The different steps in (b) and (c) have been drawn beside each other so that the tails are visible. All box sizes correspond to that in (a).

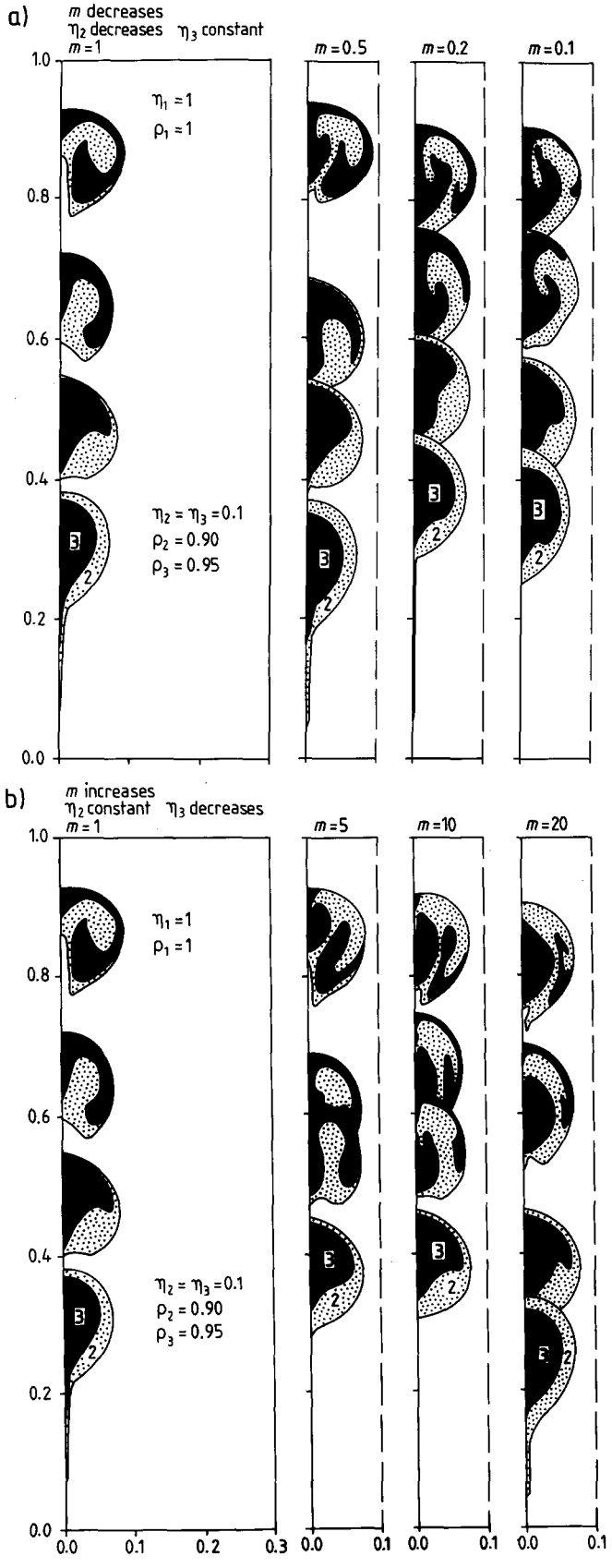
a)
m decreases
η2 decreases η3 constant
m = 1
m = 0.5
m = 0.2
m = 0.1
η1 = 1
ρ1 = 1
η2 = η3 = 0.1
ρ2 = 0.90
ρ3 = 0.95
b)
m increases
η2 constant η3 decreases
m = 1
m = 5
m = 10
m = 20
1.0
0.8
0.6
0.4
0.2
0.0
0.0
0.1
0.2
0.3

TABLE 1

Model and theoretical velocities

	m	Radius	η	ρ	v_m	B'
a	10	0.0806	0.055	0.92	0.46	0.375
b	0.1	0.0819	0.055	0.92	0.48	0.375

Parameters and velocities related to Fig. 7. All values are non-dimensional. Radius is the sphere radius as measured from the models; ρ and η are the arithmetic average density and viscosity of the spheres respectively; v_m is the non-dimensional model velocity. In order to obtain dimensional velocities, the non-dimensional values should be multiplied by $K/h = 3.3 \times 10^{-11}$ m/s, where K is thermal diffusivity (10^{-6} m^2/s), and h is the dimensional height of the model box (3×10^4 m). B' is a non-dimensional measure of buoyancy defined in the text.

dency to minimise viscous dissipation, and viscous shear caused by the sphere's rise.

The interplay of differences in both viscosity and buoyancy of the two internal fluids was studied by selecting a density contrast close to the limit of decoupling found in Fig. 4. This density contrast was kept constant while the viscosity of one of the fluids was varied. As implied by the discussion above, Fig. 6a shows that, as the viscosity of the less dense fluid *2* is decreased ($m = \eta_2/\eta_3$ decreased), the internal circulation becomes increasingly decoupled, with the lower viscosity light fluid *2* occupying the external part of the sphere. Griffiths [46] obtained very similar results in models in which fluid densities and viscosities were both composition- and temperature-dependent. His fig. 3–5 show how the denser and more viscous ambient fluid is, under some conditions, entrained in the lower core of the rising "thermal" and maintains this position throughout the rise of the thermal (decoupled internal circulation).

A surprise, however, resulted when the viscosity of the denser fluid *3* was decreased (m increased; Fig. 6b). Contrary to expectations, the less viscous fluid did not seek the external part of the sphere. Instead the circulation decoupled, with the lighter and more viscous fluid *2* occupying the external zones. Comparison of Fig. 6a and b shows that any increase in the viscosity contrast (increase or decrease in m values) increases the tendency towards decoupling of the circulation. In both cases, once the denser fluids dragged upwards by the forced circulation, the lighter fluid undergoes a Rayleigh-Taylor instability to produce internal plumes. The position of the plume migrates from the centre to the external zone of the sphere as m deviates from 1. The presence of a relatively low viscosity fluid inside the sphere thus allows the buoyancy difference between the two internal fluids to act more easily.

Velocity

In this section, rise rates of model spheres are compared to those predicted by theory (e.g. [30]). The non-dimensional model velocity (v_m) of the reference sphere (Fig. 3) was compared to the theoretical non-dimensional velocity (v_t) of a fluid drop rising through an infinite fluid (Stokes' Law, eq. (1), corrected for a two-dimensional sphere). The model sphere accelerated during the first steps of the calculations until it achieved a constant non-dimensional velocity, $v_m = 0.55$. Using the radius of the model sphere after constant velocity was attained, eq. (1) predicted a theoretical non-dimensional velocity of $v_t = 0.587$. The discrepancy observed may be attributed both to difficulties in assessing the effective radius of the model sphere (because its shape is constantly changing slightly), and to entrainment of the wall

Fig. 6. Influence of viscosity changes on the pattern of internal circulation. (a) Results for decreasing values of m (decrease in η_2). (b) Results for increasing values of m (decrease in η_3). Both variations of m result in the same change in the pattern of internal circulation from coupled (left) to decoupled (right) irrespective of which of the two fluids becomes less viscous.

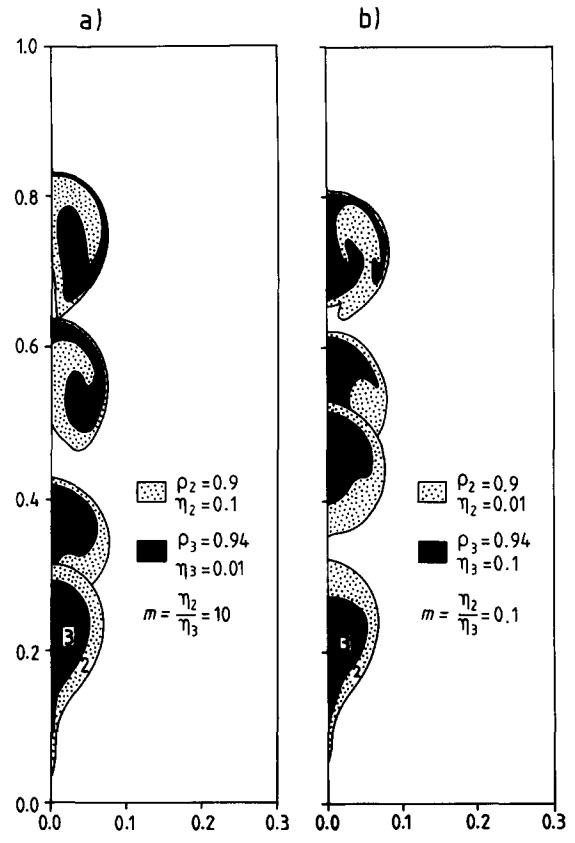

Fig. 7. Results of two calculations where $V_2 = V_3$ and the spheres have equal B' values but different m. (a) Coupled circulation. (b) Limit between coupled and decoupled circulation. These two results were used for velocity comparisons (Table 1) since both spheres have the same average density and viscosity.

rock fluid into the sphere. Similar discrepancies between calculated and measured velocities were found in all models.

Velocities were measured in two model spheres where the only difference was that the denser fluid was more viscous in one, and less viscous in the other (different m and equal buoyancy, Table 1 and Fig. 7a and b). The spheres were of equal average density and viscosity, and the two internal fluids were of equal volume. The results show that, while coupled circulation occurs in the model with $m = 10$ (Fig. 7a), the model with $m = 0.1$ (Fig. 7b) represents the limiting case between coupled and decoupled circulation. Following the initial acceleration, the constant velocities of both spheres were very similar and the small difference can be attributed to the difference in radii (Table 1). Although the change in internal viscosity distribution did not significantly affect the velocities of the sphere, it clearly controlled the development of the internal flow.

Discussion of the internal circulation

Density

The influence of density variations on the pattern of circulation within the two-fluid sphere can be summarized as follows: circulation is controlled by the relationship between the viscous shear driving the internal circulation and the buoyancy forces inside the sphere that tend to preserve a gravitationally stable internal stratification. Buoyancy forces will either enhance or hinder the rate of internal overturn, depending upon whether the stratification is initially gravitationally unstable or stable.

In order to quantify and predict the pattern of internal circulation developed by a rising two-fluid sphere, a non-dimensional parameter is defined in relation to the buoyancy forces affecting the system. Buoyancy forces have two different effects on the system considered here. One is the effect of the total buoyancy force of the sphere itself (B_t), which controls its rise velocity: $B_t = (\rho_1 - \rho_2)gV_2 + (\rho_1 - \rho_3)gV_3$. The other effect is the difference in buoyancy between the two fluids (fluids *2* and *3*) inside the sphere. The non-dimensional parameter B' describes the ratio between the buoyancy force of one of the internal fluids to the total buoyancy force:

$$B' = \frac{B_d}{B_t} = \frac{(\rho_1 - \rho_d)V_d}{B_t}g \qquad (3)$$

where B_d, r_d, and V_d are the buoyancy, density and volume, respectively, of the denser of the two fluids inside the sphere. The buoyancy of the denser of the two fluids was chosen arbitrarily as a reference (the buoyancy of the lighter fluid could equally be used). Choosing the denser (or the lighter) of the fluids, rather than fluid *2* or *3*, neglects the initial density distribution inside the sphere. The two models on the extreme right-hand side of Fig. 4a and b represent the limit between coupled and decoupled circulation and correspond to values of B' of 0.307 and 0.279, respec-

tively. The difference is due to the initial density distribution in the sphere.

Equation (2), derived by Schmeling et al. [25] for one internal overturn during the rise of an homogeneous sphere, does not apply to spheres containing two fluids with different densities. As can be seen from the decoupled cases in the right-hand side of Fig. 4, buoyancy forces will allow viscous drag to drive half an overturn at the most when $\rho_3 < \rho_2$, and no overturn whatsoever when $\rho_3 > \rho_2$. The overturn rate for cases intermediate between perfect coupled and decoupled circulations will be retarded when the less dense fluid occupies the external position in the sphere, and accelerated when it occupies the more central position.

Viscosity

Analysing the effects of viscosity variation on the pattern of internal circulation (with constant densities) allowed the empirical determination of the parameter controlling the circulation. This was found to be the viscosity ratio between the two internal fluids, $m = \eta_2/\eta_3$, that expresses the way viscous forces are transmitted between the two internal fluids. The results (Fig. 5) show that the most coupled circulation occurs when the two internal fluids have equal viscosity ($m = 1$) and their movement results in long tails, left behind as they circulate. By increasing the viscosity contrast (i.e., increasing or decreasing m) the two fluids tend to move separately and decouple and the tails become much thinner or disappear completely.

The parameter m does not take account of the viscosity of the ambient fluid *1*. In Fig. 5b the sphere's external fluid, *2*, has the same viscosity as fluid *1* ($\eta_1/\eta_2 = 1$). Fluid *2* is strongly coupled to fluid *1* and is strongly retarded in its rise forming a long tail behind the sphere. In Fig. 5c, $\eta_1/\eta_2 = 100$, fluid *2* is less retarded than in Fig. 5b and the tail is formed by the more viscous internal fluid 3 ($\eta_1/\eta_3 = 1$). These results indicate that the viscosity ratio between the ambient fluid *1* and the external of the sphere's fluids affects the internal circulation and that strong

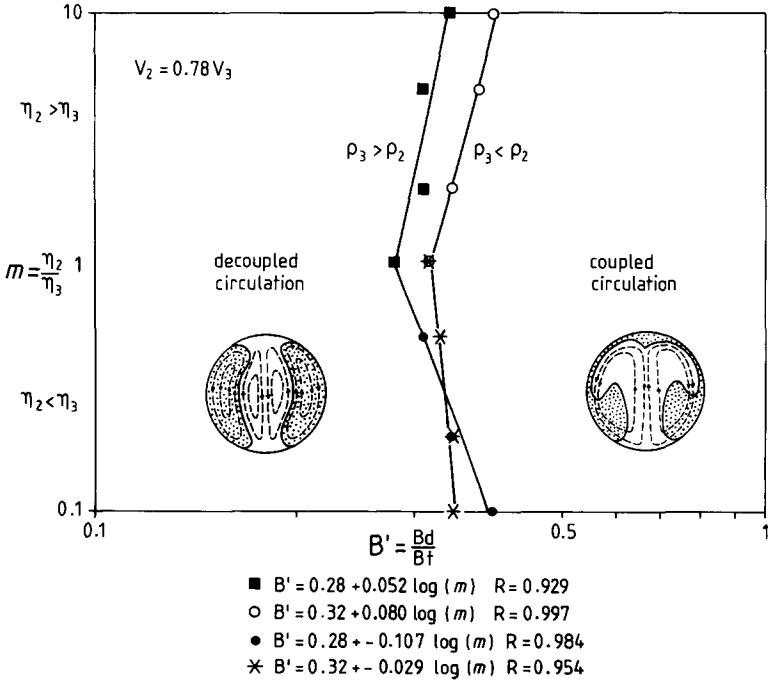

Fig. 8. Plot of m versus B' for models with $V_2 = 0.78V_3$. The boundaries of the two circulation fields shown above vary when the relative volume of the two internal fluids are varied. When the internal volumes are varied and $V_2 = V_3$ the field of coupled circulation for $\rho_3 > \rho_2$ increases due to the smaller volume of the denser fluid *3* as compared to $V_2 = 0.78V_3$. For $\rho_3 < \rho_2$, the denser fluid *2* offers more resistance to circulation than in $V_2 = 0.78V_3$ causing a decrease in the field of coupled circulation.

coupling between both these fluids ($\eta_1/\eta_{external} = 1$) enhances coupled circulation (Fig. 5). However, the influence of the viscosity of the ambient fluid at the limit between the two styles of circulation is of minor importance in comparison to m and is inherent in the equations derived below determining the limits between the circulation styles.

Integration of viscosity and density variations

Having studied how viscosity and density contrasts control the internal circulation, it is now possible to integrate the results and define the general limits between coupled and decoupled circulation inside spheres with $V_2 = 0.78V_3$. These limits were defined by systematically varying the value of ρ_3 for every value of m and finding where the first decoupled geometry develops. The results are defined in terms of the non-dimensional parameters m and B' (Fig. 8). Ninety calculations were made in order to define these limits but, since these are gradational, their exact limit is difficult to assess and causes deviation of points from the straight boundary defined. The increased dependency of the value of B' on the value of ρ_3 in calculations where $\rho_3 > \rho_2$, caused a reduced accuracy in the determination of B' limiting the fields of coupled and decoupled circulation.

As expected, the results show that the field of coupled circulation is widest for isoviscous spheres ($m = 1$ in Fig. 8). An increase or decrease in the viscosity contrast m leads towards internal decoupling. The transitional boundary for $\rho_3 < \rho_2$ moves towards higher values of B' than for $\rho_3 > \rho_2$ (Fig. 8) because of the influence of initial sphere acceleration.

Channel models

The spheres modelled above ascended through an isoviscous material sufficiently wide to approximate an infinitely wide ambient fluid (Stokes-like ascent). Daly and Raefsky [15] showed that wall rock behaving as an infinitely wide fluid is only found in diapirs rising with very high or very low Peclet numbers, that is, Pe < 5 or Pe > 100. For diapirs with Pe numbers between 5 and 100, virtually all deformation of the wall rock is confined to a narrow shear zone, with a lowered viscosity as a result of heat from the diapir. In order to model the way in which such a narrow zone influences the patterns of circulation within the diapir, the shear zone around the diapir was simplified to an isoviscous cylindrical or planar channel only slightly wider than the sphere itself. This simulates the case of several diapirs following the same pathway [12] or a magma body ascending through a low viscosity shear zone. The solution for the rise of the sphere through a cylinder [32] shows that drag on the sphere may be several orders of magnitude larger than that seen in Stokes-like flow and depends on the relative widths of the cylinder and sphere and, to a lesser extent, on the viscosity ratio between the sphere and the fluid in the cylinder (e.g., [12]). Here, the constant low viscosity channel was chosen to be only slightly wider than the initial sphere (Fig. 9b).

Circulation within a sphere rising along a narrow channel is faster than that in the Stokes-like model (Fig. 9a,b), since the viscous drag at the sphere's contact is increased by several orders of magnitude. The increase in drag is reflected by the concentration of the streamlines towards the sphere in Fig. 9b as compared to Fig. 9a. The initial spherical body deforms to an ellipsoid with a width approximately half that of the channel. This distortion is due to an increase in shearing at the sphere's side, stretching the body to minimize the viscous dissipation by drag. The elliptical shape assumed by the sphere (aspect ratio 3) may have influenced the calculations of heat transfer and body shape carried out by Marsh [12], where a roughly spherical body was assumed to rise along a cylindrical channel.

The fields of coupled and decoupled circulation could not be limited precisely in these channel models because the two fluids were stirred and disrupted into small blobs as they rose (Fig. 9b, top diagram). The computer calculations may become unreliable, due to undefined viscosity

Fig. 9. Two models with the same viscosity and density where (a) has an infinite ambient fluid and (b) has a low viscosity channel in a high viscosity (almost rigid) ambient fluid. The streamlines become concentrated closer to the sphere in (b), indicating higher shear drag. This increased drag in (b) causes faster development of internal circulation.

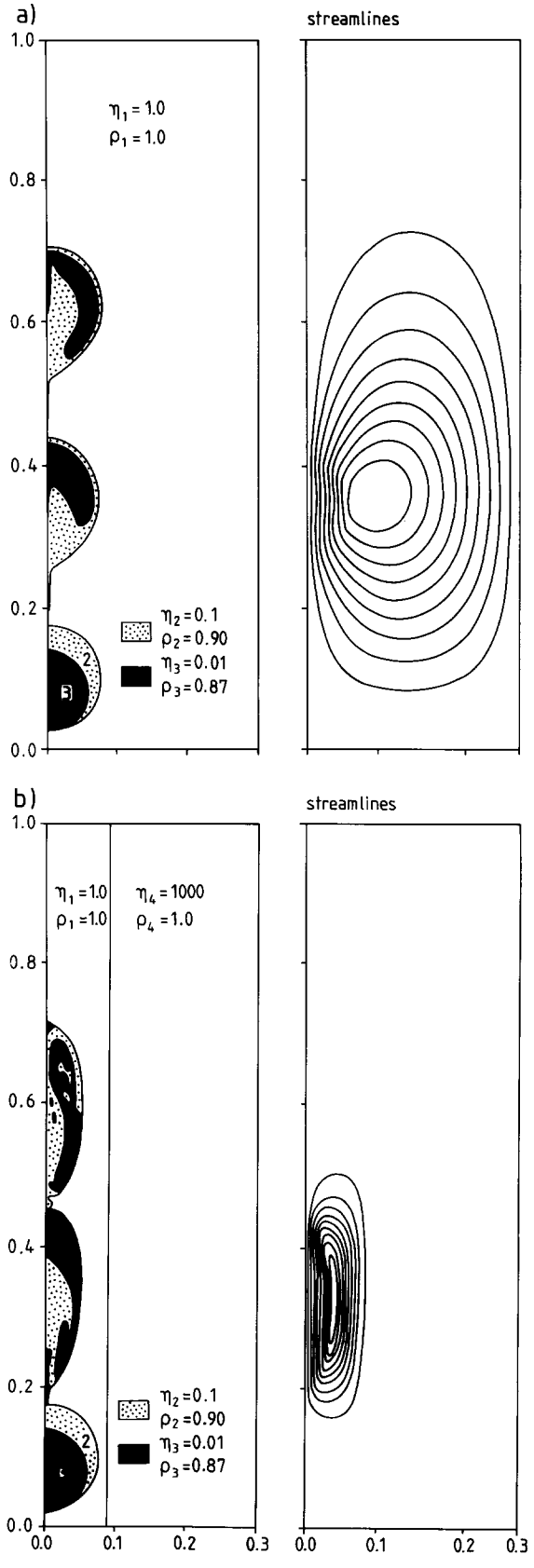
a)
streamlines
1.0
0.8
0.6
0.4
0.2
0.0
$\eta_1 = 1.0$
$\rho_1 = 1.0$
$\eta_2 = 0.1$
$\rho_2 = 0.90$
$\eta_3 = 0.01$
$\rho_3 = 0.87$
2
3
b)
streamlines
$\eta_1 = 1.0$
$\rho_1 = 1.0$
$\eta_4 = 1000$
$\rho_4 = 1.0$
$\eta_2 = 0.1$
$\rho_2 = 0.90$
$\eta_3 = 0.01$
$\rho_3 = 0.87$
0.0
0.1
0.2
0.3

caused by a lack of markers in these blobs. However, the more intense circulation suggests that coupled circulation is favoured.

The models described above imply that circulation within diapirs with Pe numbers between 5 and 100 will be faster than that in Stokes-like spheres. Faster stirring of the fluids increases the possibilities of magma mingling, mixing and eventual homogenisation. For a sphere enclosed in another sphere of low viscosity ambient fluid (diapir warming a sphere of wall rock as it rises) the viscous drag is slightly higher than for the cylinder case [12], so that internal circulation might be expected to be slightly faster than in the channel models.

Implications for magmatic diapirs

The experiments described above simulate diapirs containing two chemically distinct magmas. The closer the physical properties of the two magmas, the more coupled the circulation (*m* close to unity and/or high B'). Circulation decouples for two internal magmas with very different physical properties, that is, low B' values and/or large/small *m* values. Decoupling leads the less dense fluid to occupy the external zone of the sphere, which corresponds to plutons with reverse zoning. Coupled circulation, due to the constant overturn between the two fluids, will develop through phases of normal and reverse zoning. The final geometry depends on the stage at which circulation ceases as a result of increase in viscosities due to cooling. Any difference in the densities of the two internal fluids will favour reverse zoning (Fig. 4) because of the tendency of the lighter fluid to maintain larger volumes in the external zone for longer periods of time.

Although on the local scale thermal equilibrium may be achieved between magmas, the whole diapir may only achieve equilibrium late in its history. However, in order to predict the internal circulation in simplified magmatic systems, we assume for discussion purposes that thermal equi-

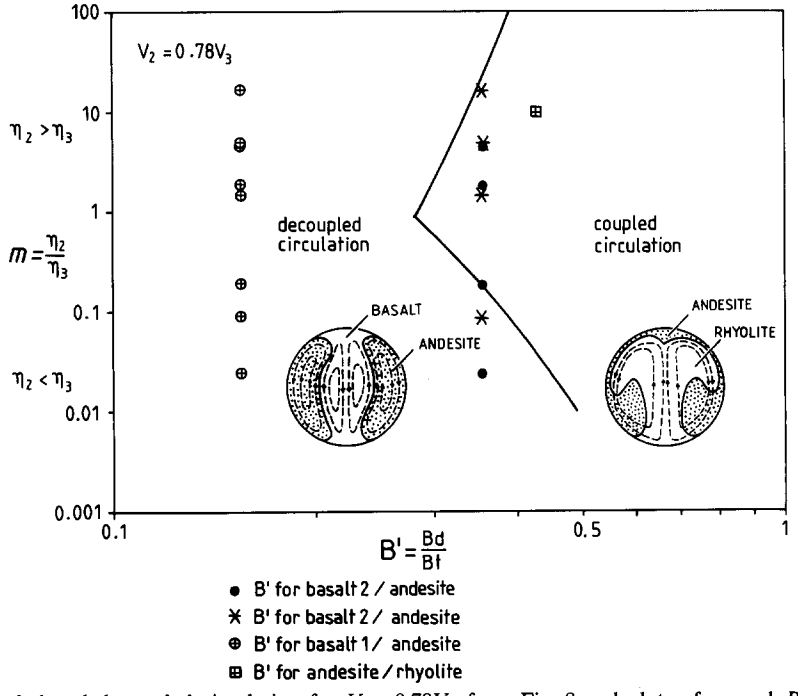

Fig. 10. Fields of coupled and decoupled circulation for $V_2 = 0.78V_3$ from Fig. 8 and plots of *m* and B' values for thermally equilibrated magmas. The values of B' are listed in Table 4 and were calculated for a crust with density 2800 kg/cm^3. The values of *m* are from Table 2 and were calculated from viscosity values for thermally equilibrated magmas as depicted from the graphs in Frost and Mahood [4] (their fig. 15 and 16) and Sparks and Marshall [17] after thermal equilibration between the magmas.

TABLE 2

$V_2 = 0.78V_3$

% H_2O Andesite	m Andesite/ Basalt 1 or 2 with 1% H_2O	m Andesite/ Dry Basalt 1 or 2	m Rhyolite/ Andesite (from [17])
1	16.9	4.6	10.2
2	4.9	1.92	
3	1.5	0.19	
5	0.09	0.024	

Values of m depicted from magma viscosities at thermal equilibration (from [4,17]) for $V_2 = 0.78V_3$ (fraction of mafic magma = 0.56). Andesite corresponds to Frost and Mahood's melt with 60% SiO_2 content and Sparks and Marshall's melt with 62% SiO_2, basalt to 50% SiO_2, and rhyolite to Sparks and Marshall's melt with 72% SiO_2. This table was used in Fig. 10.

librium is achieved early in the diapir's evolution and use the viscosity values from the graphs in Frost and Mahood [4] (their fig. 15 and 16) and Sparks and Marshall [17]. The viscosity ratios between different pairs of magmas for the volumetric proportion studied in this paper ($V_2 = 0.78V_3$) are listed in Table 2 (from [4]). The B' values for different pairs of magmas were calculated using the densities in Table 3 and are listed in Table 4. The denser mafic magma in the calculations initially occupies the centre of the sphere (fluid *3* in the models above, $\rho_3 > \rho_2$).

TABLE 3

Densities

Magma	ρ (kg/m^3)
Basalt 1	2750
Basalt 2	2650
Andesite	2450
Rhyolite	2200
Wall rock	2800

Density values used in the calculations of B' in Table 4 (from [40], except the value for the wall rock). Basalt 1 and basalt 2 are the two different basalts treated by these authors.

The values of m and B' from Tables 2 and 4 are plotted in Fig. 10, where the fields of coupled and decoupled circulation defined in Fig. 8 are

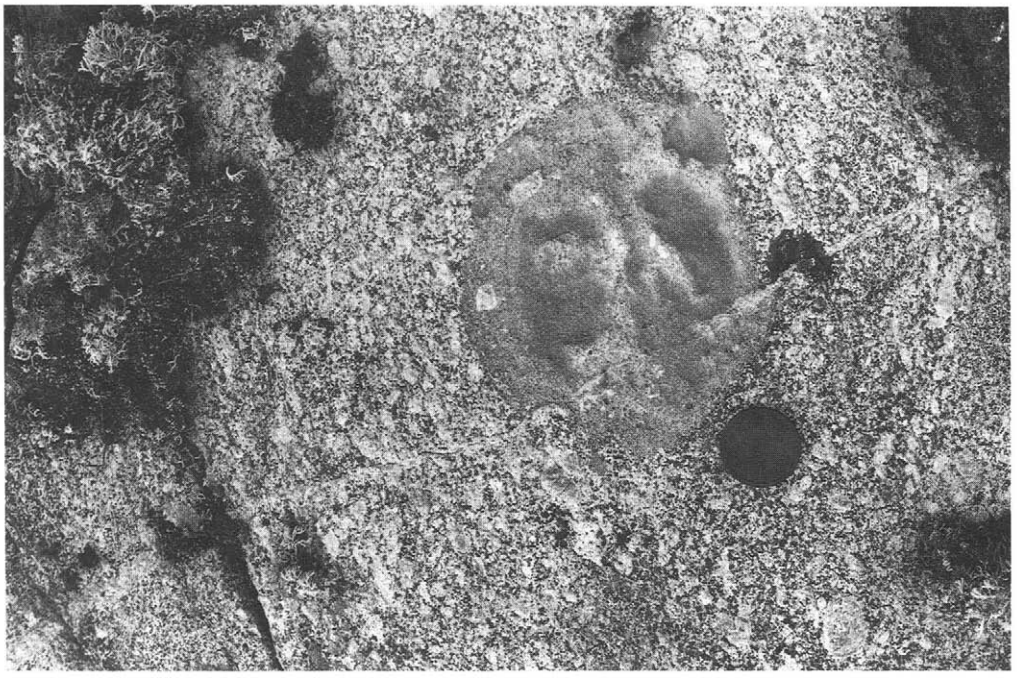

Fig. 11. Microgranitoid enclave showing frozen internal circulation patterns due to motion relative to the surrounding granite (from [49], fig. 3). The hybrid zones (grey) show circulation coupled with the unhybridised dark patches. Note the two incorporated K-feldspar phenocrysts in the hybrid zone flow-aligned along the outer contact of the enclave. The aligned feldspars in the granite indicates flow surrounding the enclave (vertical in the figure).

TABLE 4
Values of B'

Magamas	$B'(V_2 = 0.78V_3)$
Basalt 1/Andesite	0.155
Basalt 2/Andesite	0.354
Basalt 1/Rhyolite	0.097
Basalt 2/Rhyolite	0.242
Andesite/Rhyolite	0.428

Values of B' calculated for different pairs of magmas using the densities listed in Table 3.

also plotted. Figure 10 shows that coupled circulation will easily develop in diapirs formed by pairs of silica-rich magmas (e.g., rhyolite–andesite) due to their low density compared to the surrounding crust (high B'). Flow in diapirs formed by two relatively basic melts (basalt 1 or 2 and andesite) will usually decouple due to their high density compared to the enveloping crust (low B'). Nevertheless, coupling occurs in a few cases where m is close to unity and B' is relatively high. Pairs of magmas of extreme compositions (rhyolite–basalt) plot far inside the field of decoupled circulation (not shown in Fig. 10) because of both their high difference in density (low B') and the high absolute density of the basalt. In summary, the circulation within diapirs comprised of around 50% basic melt and 50% of a more acidic melt is likely to decouple and develop reverse zoning. Circulation in light diapirs formed by two felsic melts with low viscosity contrast is likely to be coupled.

Mixing of two magmas at their contact may trigger coupling by the formation of intermediate magmas (intermediate densities and viscosities). Once coupled circulation initiates, stirring of the two melts and the formation of long tails behind the circulating magmas (Fig. 5) will enhance mingling, and consequently chemical mixing, due to increase in the contact area between the mingled melts. This feedback process, where mixing and coupled circulation reinforce each other, may finally lead to complete homogenisation of the two magmas.

The patterns of internal circulation presented here may also account for magmatic spheres of much smaller scale. Inside plutonic bodies, internal circulation of small viscous spherical enclaves may be caused by relative flow to the surrounding magma thus leading to enhanced mixing (Fig. 11). In regions of the lower crust where melting occurs, magma may accumulate and form decimeter large spheres that will rise through the melting region [48]. Circulation inside these small spheres may lead to their homogenisation.

Conclusion

Two styles of internal circulation occur in two-fluid spheres depending on the relation between the viscous shear at the external boundary and the buoyancy forces inside the sphere. The circulation is coupled when the viscous shear stirring the sphere is stronger than the buoyancy forces inside it. Coupled circulation occurs only for light diapirs (in relation to the crust) with magma pairs of low viscosity contrast and low density difference. Coupling may produce both normal and reverse zoned diapiric plutons, although density differences between the two internal fluids will favour reverse zoning. Decoupled circulation is the most likely geometry of two-magma diapirs (Fig. 10) and represents the equilibrium situation attained when buoyancy forces can overpower viscous shear. Decoupling leads to stable internal stratification and reverse zoned diapirs.

Magma mixing and coupled circulation are mutually reinforcing processes which may lead to total homogenisation of the diapir. Isoviscous diapirs present the ideal conditions for both coupled circulation (shown above) and magma mixing (as concluded by [17]). In diapirs composed of magmas with a large viscosity contrast, mixing may promote coupled circulation by creating magmas with intermediate values of viscosity and density. Conversely, coupled circulation may improve conditions for mixing.

The large increase in viscous drag in spheres rising along narrow cylindrical or planar channels [32] drives internal circulation faster than spheres rising through an infinitely wide ambient fluid. Although the limits between the two styles of circulation could not be assessed, it is expected that the field of coupled circulation would increase.

The patterns of circulation and the limits between the two fields of circulation decribed here may be affected by non-Newtonian behaviour or

temperature-dependent viscosity of the magmas and crust. Similarly, disturbances may be caused by processes such as: sequential diapiric intrusion of increasingly more evolved magmas; the activity of parallel processes during or after emplacement (crystallization from the borders inwards, crystal settling, thermal convection); or even magma emplacement by mechanisms other then diapirism such as magmatic fracturing.

Acknowledgements

I wish to thank Harro Schmeling for developing and introducing me to the computer code used in this work as well as for his constructive discussion, suggestions and critical reading of the manuscript. I would also like to express my thanks to Ruud Weijermars, Christopher Talbot, Alexander Cruden, Anders Wikström and Ulf Andersson for critical reading and discussion, the latter is also thanked for lending me his photograph (Fig. 11). I thank Stefan Bergman for discussion and ideas, and the assistance of Sharon Ford for English style and Christina Wernström for preparation of the figures is gratefully acknowledged. This study was supported by a study grant from the University of Uppsala.

References

1 W. Hildreth, Gradients in silicic magma chambers: implications for lithospheric magmatism, J. Geophys. Res. 86, 10153–10192, 1981.
2 H.E. Huppert and S.J. Sparks, The generation of granitic melts by intrusion of basalt into continental crust, J. Petrol. 29, 599–624, 1988.
3 W.S. Pitcher, Granites and yet more granites forty years on, Geol. Rundsch. 76, 51–79, 1987.
4 T.P. Frost and G.A. Mahood, Field, chemical, and physical constraints on mafic–felsic magma interaction in the Lamarck Granodiorite, Sierra Nevada, California, Bull. Geol. Soc. Am. 99, 272–291, 1987.
5 P.C. Bateman and W.J. Nokleberg, Solidification of the Mount Givens granodiorite, Sierra Nevada, California, J. Geol. 86, 563–579, 1978.
6 M.P. Atherton, W.J. McCourt, L.M. Sandersson and W.P. Taylor, The geochemical character of the segmented Peruvian Coastal Batholith and associated volcanics, in: Origin of Granitic Batholiths—Geochemical Evidence, M.P. Atherton and J. Tarney, eds., pp. 45–64, Shiva Press, Orpington, 1979.
7 P.I. Nabelek, J.J. Papike and J.C. Laul, The Notch Peak Granitic Stock, Utah: origin of reverse zoning and petrogenesis, J. Petrol. 27, 1035–1069, 1986.
8 P. Bayer, R. Schmidt-Thomé, K. Weber-Diefenbach and H.A. Horn, Complex concentric granitoid intrusions in the coastal mobile belt, Espirito Santo, Brazil: the Santa Angelica pluton—an example, Geol. Rundsch. 76, 357–371, 1987.
9 J.S. Beard and H.W. Day, Petrology and emplacement of reversely zoned gabbro–diorite plutons in Smartville Complex, Northern California, J. Petrol. 29, 965–995, 1988.
10 P.C. Bateman and B.W. Chappell, Crystallization, fractionation and solidification of the Tuolomne intrusive series, Yosemite National Park, California, Bull. Geol. Soc. Am 90, 465–482, 1979.
11 M.J. Zorpi, C. Coulon, J.B. Orsini and C. Cocirta, Magma mingling, zoning and emplacement in calc-alkaline granitoid plutons, Tectonophysics 157, 315–329, 1989.
12 B.D. Marsh, On the mechanics of igneous diapirism, stoping, and zone melting, Am. J. Sci. 282, 808–855, 1982.
13 S. Morris, The effects of a strongly temperature-dependent viscosity on slow flow past a hot sphere, J. Fluid Mech. 124, 1–26, 1982.
14 N. Ribe, Diapirism in the Earth's mantle: experiments on the motion of a hot sphere in a fluid with temperature dependent viscosity, J. Volcanol. Geotherm. Res. 16, 221–245, 1983.
15 S.F. Daly and A. Raefsky, On the penetration of a hot diapir through a strongly temperature-dependent viscosity medium, Geophys. J.R. Astron. Soc. 83, 657–681, 1985.
16 S. Cruden, Deformation around a rising diapir modelled by creeping flow past a sphere, Tectonics 7, 1091–1101, 1988.
17 R.S.J. Sparks and L.A. Marshall, Thermal and mechanical constraints on mixing between mafic and silicic magmas, J. Volcanol. Geotherm. Res. 29, 99–124, 1986.
18 F.F. Grout, Scale models of structures related to batholiths, Am. J. Sci. 243, 260–284, 1945.
19 H. Ramberg, Gravity, Deformation and the Earth's Crust in Theory, Experiments and Geological Application, 452 pp., Academic Press, London, 2nd ed., 1981.
20 H. Ramberg, Model studies in relation to plutonic bodies, in: Mechanism of igneous intrusion, A. Newall and N. Rast, ed., Geol. J. Spec. Issue 2, 261–286, 1970.
21 G.K. Batchelor, An Introduction to Fluid Dynamics, 615 pp., Cambridge University Press, London, 1967.
22 J.A. Whitehead and D.S. Luther, Dynamics of laboratory diapirs and plume models, J. Geophys. Res. 80, 705–717, 1975.
23 H. Berner, H. Ramberg and O. Stephansson, Diapirism in theory and experiment, Tectonophysics 15, 197–218, 1972.
24 W.D. Woidt and H.J. Neugebauer, Finite-element models of density instabilities by means of bicubic spline interpolation, Phys. Earth Planet. Inter. 21, 176–180, 1980.
25 H. Schmeling, A.R. Cruden and G. Marquart, Finite deformation in and around a fluid sphere moving through a viscous medium: implications for diapiric ascent, Tectonophysics 149, 17–34, 1988.
26 R. Bateman, On the role of diapirism in the segregation, ascent and final emplacement of granitoid magmas, Tectonophysics 110, 211–231, 1984.
27 K.I. Mahon, T.M. Harrison and D.A. Drew, Ascent of a

granitoid diapir in a temperature varying medium, J. Geophys. Res. 93, 1174–1188, 1988.
28 H.R. Shaw, Rheology of basalt in the melting range, J. Petrol. 10, 510–535, 1969.
29 H.R. Shaw, Viscosities of magmatic silicate liquids: an empirical method of prediction, Am. J. Sci. 272, 870–893, 1972.
30 J. Hadamard, Mouvement permanent lent d'une sphere liquide et visqueuse dans un liquid visqueux, C.R. Acad. Sci. 152, 1735–1738, 1911.
31 W. Rybczynski, Über die fortschreitende Bewegung einer flüssigen Kugel in einen zähen Medium, Bull. Acad. Sci. Cracovie 1, 40–46, 1911.
32 J. Happel and H. Brenner, Low Reynolds Number Hydrodynamics, 553 pp., Martinus Nijhoff, Dordrecht, 1986.
33 K.E. Spells, A study of circulation patterns within liquid drops moving through a liquid, Proc. Phys. Soc. B65, 541–546, 1952.
34 R.W. Griffiths, Particle motions induced by spherical convective elements in Stokes flow, J. Fluid Mech. 166, 139–159, 1986.
35 A.R. Cruden, Flow and fabric development during the diapiric rise of magma, J. Geol. 98, 681–698, 1990.
36 R.A. Wiebe, Commingling of contrasted magmas in the plutonic environment: examples from the Nain Anorthositic Complex, J. Geol. 88, 197–209, 1980.
37 R. Weijermars and H. Schmeling, Scaling of Newtonian and non-Newtonian fluid dynamics without inertia for quantitative modelling of rock flow due to gravity (including the concept of rheological similarity), Tectonophysics 124, 325–358, 1986.
38 G.R. Robson, Thickness of the Etnean lavas, Nature 216, 251–252, 1967.
39 A.R. McBirney and T. Murase, Rheological properties of magmas, Annu. Rev. Earth Planet. Sci. 12, 337–357, 1984.
40 T. Murase and A.R. McBirney, Properties of some common igneous rocks and their melts at high temperatures, Geol. Soc. Am. Bull. 84, 3563–3592, 1973.
41 I. Van der Molen and M.S. Paterson, Experimental deformation of partially melted granite, Contrib. Mineral. Petrol. 70, 299–318, 1979.
42 S.H. Kirby, Rheology of the lithosphere, Rev. Geophys. Space Phys. 21, 1458–1487, 1983.
43 H. Ramberg, The stream function and Gauss' principle of least constraint: two useful concepts for structural geology, Tectonophysics 131, 205–246, 1986.
44 R.F. Weinberg and H. Schmeling, Polydiapirs: Multiwavelength gravity structures, J. Struct. Geol., in press, 1992.
45 B.D. Marsh and M.R. Maxey, On the distribution and separation of crystals in convecting magma, J. Volcanol. Geotherm. Res. 24, 95–150, 1985.
46 R.W. Griffiths, The differing effects of compositional and thermal buoyancies on the evolution of mantle diapirs, Phys. Earth Planet. Int. 43, 261–273, 1986.
47 D.D. Joseph, K. Nguyen and G.S. Beavers, Non-uniqueness and stability of the configuration of flow of immiscible fluids with different viscosities, J. Fluid Mech. 141, 319–345, 1984.
48 W.S. Fyfe, The generation of batholiths, Tectonophysics 17, 273–283, 1973.
49 U.B. Andersson, Granitoid episodes and mafic–felsic magma interaction in the Svecofennian of the Fennoscandian Shield, with main emphasis on the ≈ 1.8 Ga plutonics, Precambrian Res. 51, 127–149, 1991.